Iranian Journal of Polymer Science and Technology Vol 4 No 2 (1995)

Measurement of Adhesion and Interfacial Thickness of Polymer-Polymer Interfaces with Electron Microscopy

Esmaiel Jabbari* and Nicholas A. Peppas
School of Chemical Engineering
Purdue University
West Lafayette, Indiana 47907 - 1283, USA

Received: 7 May 1994; accepted 28 December 1994

ABSTRACT

The interfacial thickness of polymer-polymer bilayers is determined by the concentration profile of the two polymers across the interface. After intimate contact is established between two polymer films, adhesion takes place by interdiffusion of polymer chains across the interface. The combination of transmission electron microscopy and energy dispersive spectroscopy (TEM/EDS) is used to map the concentration profile at the interface of a poly (vinyl chloride) and poly (methyl methacrylate) bilayer. Thin sections in the order of 800 Å are cut using an ultramicrotome, examined with TEM, and the concentration profile is mapped with EDS. The intensity of x-ray fluorescence is adjusted for variation in sample thickness by measuring the relative thickness across the interface with electron energy-loss spectroscopy (EELS). The interfacial thickness of the bilayer after 6 hours at 120 °C was 1.5 μm. The concentration profile is fitted to the Ficklan diffusion equation and an average interdiffusion coefficient of 8.0×10^{-14} cm^2/s is obtained in good agreement with values reported in the literature.

Key Words

poly (vinyl chloride), poly(methyl methacrylate), interdiffusion, interface, electron microscopy

INTRODUCTION

Interdiffusion at the interface between polymer-polymer bilayers affects the interfacial thickness and mechanical properties of these interfaces [1-4]. Applications include welding of polymer interfaces in processing of powder and pellet resins [5, 6], internal weld lines of multicomponent polymer melts in coextrusion and injection molding [7-9], lamination of composites [10,11], latex film formation in paints and coatings [12], diffusion-controlled reactions of polymers [13, 14], and bioadhesion [15-17].

In the fabrication of microelectronic devices, adhesion of polyimide-polyimide layers in the passivation stage and of polyimide-epoxy layers in

* Present address: Dept of Polymer Engineering , Amir Kabir University of Technology, Tehran 15914, Iran.

the encapsulation stage is crucial to protect the chip from gamma rays and moisture [18-20]. In packaging of food products, the performance of the laminated structure, consisting of an oxygen barrier layer sandwiched between two moisture barrier layers, is controlled by the adhesion and bond strength of the oxygen and moisture barrier layers [9]. In paints and coatings, polymer interdiffusion and autohesion at the boundaries of latex particles yield a homogeneous film [12]. In biomedical applications, the adhesion of hydrogel, as the drug carrier, to mucus, as the biological substrate, is important for controlled release of drugs in nasal, buccal, and sublingual administration [21].

Stages of polymer-polymer diffusion at an interface include intimate contact, wetting, and chain interpenetration. Intimate contact and wetting play an important role in the initial phase of polymer-polymer adhesion. After intimate contact is established between two polymer films, adhesion takes place by interdiffusion of polymer chains across the interface [1] with the extent of adhesion depending on the compatibility parameter between the two polymers [22]. For incompatible polymers, the interfacial thickness is of the order of angstroms whereas for compatible polymers, it is of the order of microns.

Diffusion at polymer interfaces have been examined extensively with techniques such as neutron reflectometry [23], small-angle neutron scattering [24], forward recoil spectrometry [25], secondary ion mass spectrometry [26], scanning electron microscopy [27], optical Schlieren spectrometry [28], infrared spectroscopy [29], scanning infrared microscopy [30], ellipsometry [31] and Raman scattering [32]. Of these techniques, only electron microscopy allows visual observation of the interface to directly map the concentration profile along the interfacial region. Combination of scanning electron microscopy and energy-dispersive spectroscopy (SEM/EDS) has been used to map the concentration profile across the interface between poly (vinyl chloride) (PVC) and poly(ε-caprolactone). The major disadvantages are the limited spatial resolution for polymers due to the large interaction area between the electron beam and the sample and the uncertainty in the penetration depth of the beam across the interface caused by the difference in electron density between the two polymers.

Recent studies on morphology of copolymers with transmission electron microscopy (TEM) [33] showed the superior spatial resolution of TEM compared to SEM. In a previous paper [34], we used a combination of TEM and EDS to map the concentration profile across a PVC and poly(ethyl methacrylate) (PEM) interface with enhanced spatial resolution of 100 nm compared to SEM which was in the order of 1 μm. In the previous study, we observed that the thickness of the bilayer film varied across the interface after sectioning due to the differences in viscoelastic properties of the two polymers. Here, we report on the use of TEM/EDS in combination with electron energy-loss spectroscopy (EELS) to map the concentration profile and measure interdiffusion at a polymer-polymer interface. EELS was used to measure the relative thickness of the bilayer across the interface for determination of interdiffusion coefficient. A polymer pair with complementary mechanical properties consisting of PVC and poly(methyl methacrylate) (PMMA) was used in this investigation.

EXPERIMENTAL

The PVC and PMMA samples were obtained from Scientific Polymer Products (Ontario, NY) as a secondary standard. Differential scanning calorimetry (DSC2910, TA instruments, Willmington, DE) was used for measuring the glass transition temperature, T_g, of the polymers at a scanning rate of 10°C /min. The T_g of the PVC and PMMA samples were 84 and 118°C, respectively. Gel permeation chromatography (GPC model 6000A, Waters Associates, Milford, MA) was used to measure the molecular weight and molecular weight distribution of the samples. The experiments were carried out with tetrahydrofuran (THF) as the mobile phase, μstyragel columns with

10^6, 10^5, 10^4, and 10^3 Å pore sizes were used as the stationary phase, and the flow rate was 1 mL/min. The PVC and PMMA samples had a $\overline{M}_w$ of 1.22×10^5 and 1.01×10^5 with polydispersity index of 2.1 and 2.0, respectively. The PVC and PMMA films were cast on silicon wafers from 6 wt% and 4 wt% THF and methyl ethyl ketone solutions, respectively. As a stabilizer, 1 wt% of di-n-octyltin-5,5'-bis (iso-octylmercaptoacetate) (Atochem North America, Philadelphia, PA) was added to PVC. The T_g of PVC after addition of the stabilizer was 74 °C.

The following procedure was adapted for drying the polymer films quickly with no bubble formation: one week at room temperature, then vacuum oven with the time-temperature cycle one week at room temperature, two days at 45 °C, one day at 55 °C, one day at 70 °C and finally 1 hour above the T_g of each polymer. This time- temperature cycle insured the removal of all the solvent, monitored with differential scanning calorimetry, without the formation of any bubbles inside the film. The surface roughness of the polymer films was examined perpendicular to the interface with a profilometer (Alpha step 200, Tencor Instruments, Mountain Viw, CA). The stylus tip radius was 5 μm and the stylus force was 4 mg. After drying, the two polymer films were brought in contact, placed between two microscope slides, sandwiched between two steel plates and placed in the vacuum oven preheated above the T_g of the two polymers. The steel plates served as a constant temperature heat source for controlling temperature during the experiment. Samples from the bilayer were removed from the vacuum oven as a function of time for analysis.

The interface between the two films was exposed by fracturing at liquid nitrogen temperature and embedded in an epoxy matrix for microtoming. The embedded sample was microtomed with a glass knife at room temperature to reduce the surface roughness to less than 0.2 μm. Then, thin sections in the order of 800 Å were cut using an ultramicrotome with a diamond knife at room temperature. The surface roughness after trimming was of the order of 20 Å. The sections were picked up from the surface of the water in the boat attached to the diamond knife, placed on a 100 mesh copper grid and examined in the transmission electron microscope (JOEL 2000FX, Analytical Electron Microscope) with an energy dispersive x-ray spectrometer (AN10000, Link Analytical EDS) using an accelerating voltage of 200 kV. The duration of electron bombardment at each point during the scan was 30 seconds. The chlorine atom of PVC was used as a label to map the concentration profile of PVC across the interface. The x-ray intensity was integrated over the K_α and K_β bands of chlorine and was set proportional to the PVC concentration as a function of spatial position. The x-ray intensities were corrected for variation in sample thickness with electron energy-loss spectroscopy (666 Gatan Parallel EELS) with an accelerating voltage of 200 kV.

Data Analysis

The emitted photon energy from the chlorine atoms of PVC was used to map the concentration of chlorine across the polymer-polymer interface which was directly proportional to the molar concentration of PVC. The number of x-ray counts occurring at a given energy is proportional to the number of atoms in the irradiated volume from which the x-rays originated. The detected count rate per unit interaction volume is [35]:

$$N = J_e \, Q_k \, \omega_k \, \eta_d \, n/V \qquad (1)$$

Here, N is the detected count rate of K_α and K_β x-rays, J_e is the electron flux which is a function of the materials used, Q_k is the ionization cross section for K shell excitation, ω_k is the fluorescence yield of K shell x-rays, ηd is the detector efficiency, n is the number of chlorine atoms and V is the interaction volume between the beam and the sample. The intensity of x-ray fluorescence is calculated by integrating the detected count rate over the energy band for K_α and K_β x-rays and over the interaction volume:

$$I(x) = \frac{\int\int N(\varepsilon, x) P(V) \partial\varepsilon \partial V}{V} \qquad (2)$$

Here, I(x) is the intensity of x-rays at distance x from the interface per unit interaction volume and ε is the width of the K_α and K_β energy bands. The function P(V) is the spread function of the beam inside the sample which makes the concentration profile more diffuse than the actual profile. Ideally, P(V) should be decreased to a delta function to arrive at the actual concentration profile but the interaction between the electron beam and the sample causes the incident beam to scatter into a pear shaped volume. For polymers which have a lower atomic number compared to metals, there is less elastic collision with the matrix atoms and the lateral spread of the beam is in the order of 2-3 μm. This explains the low resolution of SEM for measuring the concentration profile for polymeric materials. On the other side, for TEM in which the bilayer thickness is in the order of 800 Å the interaction volume is limited by the aperture size of the electron beam. Therefore, for thin sections, the spread function P(V) becomes unity and equation (2) reduces to:

$$I(x)= \int\int N(\varepsilon,x)\partial\varepsilon\partial V/V=I_m(x)/V \qquad (3)$$

Here, I_m (x) is the measured intensity of x-rays. For thin sections, the interaction volume becomes cylindrical with the same cross sectional area as the electron beam aperture, A_o, and length equal to sample thickness, δ. For polymer bilayers, the intensities can be normalized based on the intensities from each polymer phase far from the interface. Therefore, the normalized concentration profile is related to the x-ray intensity by:

$$\psi(x)=\frac{C(x)-C_\circ}{C_1-C_\circ}=\frac{I(x)-I_\circ}{I_1-I_\circ} \qquad (4)$$

Here, $\psi(x)$ is the normalized concentration and C(x) is the concentration at distance x from the interface. The subscripts 1 and 0 refer to positions far away from the interface on the PVC and PMMA side, respectively. For constant aperture size, the normalized concentration reduces to:

$$\psi(x)=\frac{\delta_1}{\delta(x)}\,\frac{I_m(x)-I_{m,\circ}(\delta(x)/\delta_\circ)}{I_{m,1}-I_{m,\circ}(\delta_1/\delta_\circ)} \qquad (5)$$

Here, I_m is the measured x-ray intensity and $\delta(x)$ is the sample thickness as a function of distance along the interface.

Electron energy loss spectroscopy was used to measure the sample thickness along the interface. EELS can reveal the energy distribution of electrons which have been transmitted through the sample. Figure 1 shows a typical EELS spectrum obtained from an arbitrary position across the PVC/PMMA bilayer at 200 k_eV accelerating voltage. The peak at zero energy-loss is due to electrons that have been transmitted through the sample with no loss in energy. The peak at approximately 20 eV of energy loss is the plasmon peak produced by the interaction of the beam with free electrons in the specimen, known as plasmon excitation [36]. The plasmon peak provides an accurate method to measure the sample thickness. The probability of an electron exciting n plasmons is given by [36]:

$$E(n)= (1/n!)\,(\delta(x)/\lambda_p)^n e^{\frac{-\delta(x)}{\lambda_p}} \qquad (6)$$

Here, $\delta(x)$ is the sample thickness as a function of distance from the interface and λ_p is the plasmon mean free path. Thus, the ratio of the probabilities of exciting no plasmon and one plasmon, E(0) and E (1), is given by:

$$\frac{E(1)}{E(0)}=\frac{\delta(x)}{\lambda_p} \qquad (7)$$

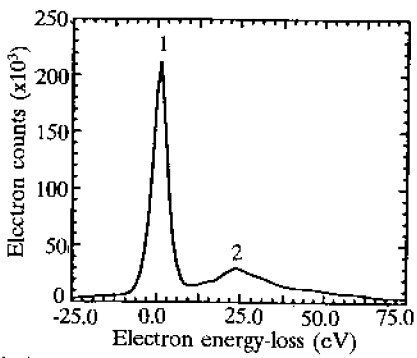

(Peaks 1 and 2 correspond to the zero-loss and plasmon peaks, respectively.)

Fig. 1. EELS spectrum of PVC/PMMA interface.

The ratio of the probabilities E(1) and E(0) is the intensity of the plasmon peak, I_P, to the zero-loss peak, I_{ZL}. Therefore, the sample thickness is given by:

$$\delta(x)=\lambda_P\frac{I_P}{I_{ZL}} \qquad (8)$$

The plasmon mean free path is related to the concentration of free electrons in the specimen and can be regarded as a constant for polymers. Therefore, equation (8) provides an accurate way to measure the relative thickness of the sample as a function of distance from the interface, x.

RESULTS AND DISCUSSION

After casting the films on silicon wafers and drying, the surface roughness of the polymer films was examined in the direction parellel to the interface with profilometry. The surface roughness of the PVC and PMMA films was less than 100 Å, as shown in Figure 2 for the PVC film. Thin sections of the polymer bilayer were cut and examined with TEM. Figure 3 shows the TEM micrograph of the PVC/PMMA interface after 6 hours at 120 °C at 1500X magnification. The top and bottom regions of the micrograph correspond to the PVC and PMMA sides of the bilayer, respectively. The position of the interface is marked by the arrow. According to this micrograph, the PMMA side of the interface is ridged with shallow and dark regions indicating that the thickness of the bilayer varies with distance across the interface. This is due to the differences in viscoelastic properties of the two polymers when the sample is sectioned.

Figure 4 shows the TEM micrograph of the PVC/PMMA interface in Figure 3 at higher magnification of 8000X. The dark circular dots in the micrograph are the locations across the interface where x-rays were collected. Chlorine x-ray counts as a function of distance for beam aperture diameters of 100 nm and 250 nm are shown in Figure 5. According to this Figure, the number of x-ray counts increased in proportion to the diameter of beam aperture verifying that the

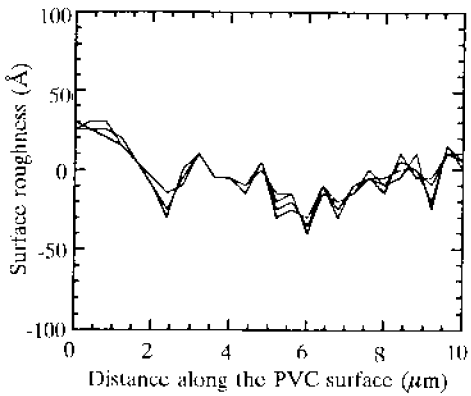

($\bar{M}_w$ of PVC was 1.22×10^5 with polydispersity index of 2.1.)

Fig. 2. Surface roughness of the PVC film parallel to the PVC/PMMA interface.

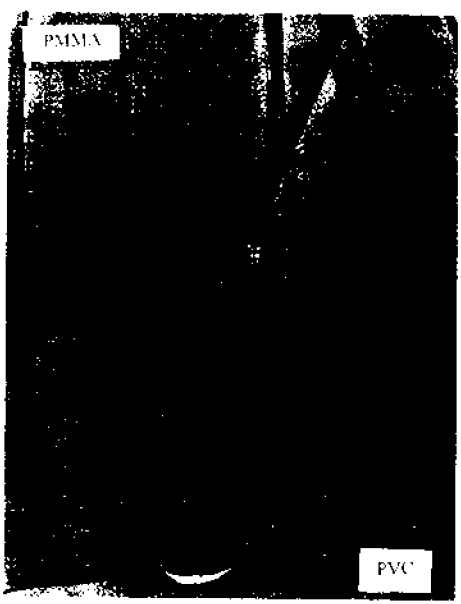

(The position of the interface is shown by the arrow. The PVC and PMMA samples had a $\bar{M}_w$ of 1.22×10^5 and 1.01×10^5 with polydispersity index of 2.1 and 2.0 respectively.)

Fig. 3. TEM micrograph of the PVC/PMMA interface at 1500X after 6 hours at 120 °C.

The PVC and PMMA samples had a $\bar{M}_w$ of 1.22×10^5 and 1.01×10^5 with polydispersity index of 2.1 and 2.0, respectively.)

Fig. 4. TEM micrograph of the PVC/PMMA interface at 8000X after 6 hours at 120 °C. The position of the interface is shown by the arrow. The dark circular bullets in the micrograph are the locations across the interface where x-rays were collected.

interaction volume is controlled by the beam diameter for thin sections. EELS was used to correct the number of x-ray counts for sample thickness. Figure 6 shows the relative thickness of the sample as a function of distance along the interface. The thickness of the PMMA side of the interface was approximately 20 percent less than the PVC side. The x-ray counts in Figure 5 were adjusted for sample thickness using equation (8) and normalized using equation (5). Figure 7 shows the normalized concentration profile for PVC/PMMA after 6 hours at 120°C. After 6 hours, the concentration profile was diffuse but the interface was symmetric with approximately 1.5 μm in thickness. The data in Figure 7 were fitted to the Fickian diffusion equation:

$$\psi = \frac{1}{2} \operatorname{erfc} \frac{x}{2\sqrt{Dt}} \tag{9}$$

Here, x is the distance from the interface, t is time and D is the interdiffusion coefficient. The diffusion coefficient is related to the slope of the concentration profile at the interface by:

$$D = \frac{1}{16t(\delta\psi/\delta\chi\,|_{x=0})^2} \tag{10}$$

Using equation (10), an interdiffusion coefficient of 8.0×10^{-14} cm^2/s was obtained for the concentration profile in Figure 7 which agrees closely with the values reported in the literature for interdiffusion in bulk polymers [37].

CONCLUSION

The concentration profile and interfacial thickness of a poly(vinyl chloride) and poly(methyl methacrylate) bilayer were measured with transmission electron microscopy and energy dispersive spectroscopy. Due to the differences in

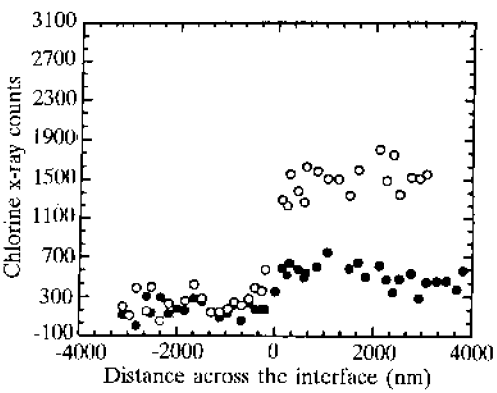

The PVC and PMMA samples had a $\bar{M}_w$ of 1.22×10^5 and 1.01×10^5 with polydispersity index of 2.1 and 2.0, respectively.)

Fig. 5. Normalized chlorine x-ray intensity across the interface for PVC/PMMA after 6 hours at 120 °C. The open and filled circles correspond to aperture diameter of 250 and 100 nm, respectively.

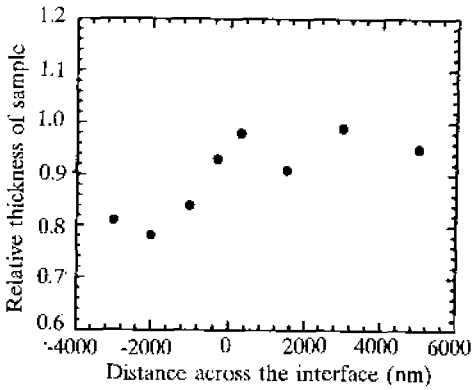

(The PVC and PMMA samples had a $\overline{M}_w$ of 1.22×10^5 and 1.01×10^5 with polydispersity index of 2.1 and 2.0, respectively.)

Fig. 6. Relative thickness of the PVC/PMMA bilayer across the interface.

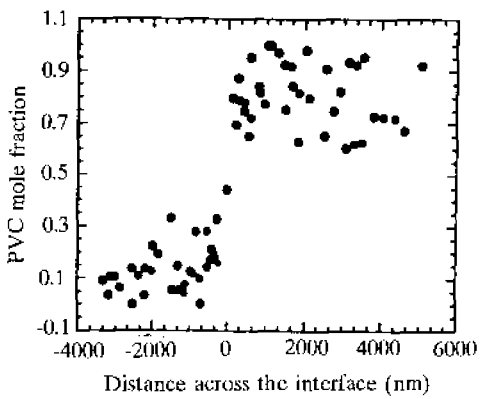

(The PVC and PMMA samples had a $\overline{M}_w$ of 1.22×10^5 and 1.01×10^5 with polydispersity index of 2.1 and 2.0, respectively.)

Fig. 7. PVC mole fraction across the PVC/PMMA interface after 6 hours at 120 °C, corrected for sample thickness variation.

viscoelastic properties of the two polymers, there was significant variation in sample thickness across the interface. Therefore, electron energy-loss spectroscopy was used to measure the relative sample thickness. The interfacial thickness after 6 hours at 120 °C was 1.5 μm. The concentration profile was fitted to the Fickian diffusion equation and an interdiffusion coefficient of 8.0×10^{-14} cm^2/s was obtained.

SYMBOLS

C(x) Concentration at distance x from the interface
D Interdiffusion coefficient
E(n) Probability of an electron exciting n plasmons
I(x) Intensity of x-rays at distance x from the interface per unit interaction volume
$I_m(x)$ Measured intensity of x-rays at distance x from the interface
I_p Intensity of the plasmon peak
I_{ZL} Intensity of the zero-loss peak
J_e Electron flux
N Detected count rate per unit interaction volume
P Spread function of the electron beam inside the sample
Q_k Ionization cross section for K shell excitation
V Interaction volume between the electron beam and the sample
n Number of chlorine atoms
x Distance from the interface
t Interdiffusion time
$\delta(x)$ Sample thickness at distance x from the interface
λ_p Plasmon mean free path
η_d x-ray detector efficiency
ω_k Fluorescence yield of K shell x-rays
$\psi(x)$ Normalized concentration of PVC at distance x from the interface
Subscript " o ": Distance far away from the interface on the PMMA side
Subscript " 1 ": Distance far away from the interface on the PVC side

REFERENCES

1 Voyutskii, S.S., *J.Adhesion*, **3**, 69 (1971).
2 Voyutskii, S.S., Autohesion and Adhesion of High Polymers, Wiley, New York, (1963).

3 Kausch, H.H., and Petrovska, D., *Polym. Prepr.*, **26**(2), 136 (1985).
4 Jud, K., Kausch, H.H., and Williams, J.G., *J. Mater. Sci.*, **16**, 204 (1981).
5 Wool, R.P., Yuan, B.-L., and Mc Garrel, *O.J., Polym. Eng. Sci.*, **29**, 1340 (1989).
6 Wool, R.P., and O'Conner, K.M., *J. Appl. Phys.*, **52**, 5953 (1981).
7 Kim, J.K., and Han, C.D., *Polym. Eng. Sci.*, **31**, 258 (1991).
8 Robeson, L.M., *Polym. Eng. Sci.*, **24**(8), 587(1984).
9 Pucci, M., Jachee, K., Machonis, J., and Shida, M., *J. Plast. Film. Sheet.*, **7**, 24 (1991).
10 Simpson, R., and Selke, S., *Polym. Prepr.*, **33** (1), 148 (1992).
11 Foster, R.H., *Polym. Prepr.*, **33**, 154 (1992).
12 Juhue, D., and Lang, J., *Macromolecules*, **27**, 695 (1994).
13 Kausch, H.H., and Tirrell, M., *Ann. Rev. Mater, Sci.*, **19**, 341 (1989).
14 El-Begawy, S.E.M., and Huglin, M.B., *Eur. Polym. J.*, **27**, 1023 (1991).
15 Gurny, R., and Junginger, H.E., Wissenschaftliche Verlagsgesellschaft, Stuttgart, (1990).
16 Peppas, N.A., and Mikos, A.G., *S.T.P. Pharma*, **5**, 187 (1989).
17 Park, H., and Robinson, J.R., *Pharm. Res.*, **4**, 457 (1987).
18 Wong, C.P., *Adv. Polym. Sci.*, **84**, 63 (1988).
19 Soane, D.S., and Mantynenko, Z., Polymers in Microelectronics: Fundamentals and Applications, Elsevier, Amsterdam, p. 153 (1989).
20 Saenger, K.L., Tong, H.M., and Haynes, R.D., *J.Polym. Sci.: Polym. Lett.*, **27**, 235 (1989).
21 Baier, R.E., *J. Biomed. Mater. Res.*, **16**, 173 (1982).
22 de Gennes. P.G., *C. R. Acad. Sci. Paris*, Serie B, **21**, 219 (1980).
23 Karim, A., Felcher, G.P., and Russell, T.P., *Polym. Prepr.*, **31**(2), 69 (1990).
24 Roland, C.M., and Bohm, G.G.A., *Macromolecules*, **18**, 1310 (1985).
25 Bruder, F., Brenn, R., Stuhn, B., and Strobl, G.R., *Macromolecules*, **22**, 4434 (1989).
26 Whitlow, S.J., and Wool, R.P., *Macromolecules*, **22**, 2648 (1989).
27 Price, F.P., Gilmore, P.T., Thomas, E.L., and Laurence, R.L., *J. Polym. Sci.: Polym. Symp.*, **63**, 33 (1978).
28 Ye, M., Composto, R.J., and Stein, R.S., *Macromolecules*, **23**, 4830 (1990).
29 Jabbari, E., and Peppas, N.A., *Macromolecules*, **26**, 2175 (1993).
30 Seggern, J.V., Klotz, S., and Cantow, H.-J., *Macromolecules*, **22**, 3328 (1989).
31 Sauer, B.B., and Walsh, D.J., *Macromolecules*, **24**, 5948 (1991).
32 Hong, P.P., Boerio, F.J., Clarson, S.J., and Smith, S.D., *Macromolecules*, **24**, 4770 (1991).
33 Koizumi, S., Hasegawa, H., and Hashimoto, T., *Macromolecules*, **23**, 2955 (1990).
34 Jabbari, E., and Peppas, N.A., *Polym. Bull.*, **27**, 305 (1991).
35 Joy, D.C., Romig, A.D., and Goldstein, J., Principles of Analytical Electron Microscopy, Plenum Press, New York, N.Y., p.53, (1986).
36 Joy, D.C., The Basic Principles of EELS, in Principles of Analytical Electron Microscopy (D.C. Joy, A.D. Romig, and J.I. Goldstein, eds.) Plenum Press, New York, N.Y., p.249 (1986).
37 Gilmore, P.T., Falabella, R., and Laurence, R.L., *Macromoleculs*, **13**, 880 (1980).